Inorg. Chem. **2006**, *45*, 5911–5923

Deliberate Synthesis for Magnetostructural Study of Linear Tetranuclear Complexes $B^{III}Mn^{II}Mn^{II}B^{III}$, $Mn^{III}Mn^{II}Mn^{II}Mn^{III}$, $Mn^{IV}Mn^{II}Mn^{II}Mn^{IV}$, $Fe^{III}Mn^{II}Mn^{II}Fe^{III}$, and $Cr^{III}Mn^{II}Mn^{II}Cr^{III}$. Influence of Terminal Ions on the Exchange Coupling

Sumit Khanra, Thomas Weyhermüller, Eckhard Bill, and Phalguni Chaudhuri*

Max-Planck-Institut für Bioanorganische Chemie, Stiftstrasse 34-36, D-45470 Mülheim an der Ruhr, Germany

Received March 10, 2006

As part of an ongoing effort to deliberate synthesis of polynuclear heterometal complexes, we are exploring synthetic routes to high-nuclearity complexes using "metal oximates" as building blocks. Series of tetranuclear linear complex ions of the general types $M_AM_BM_BM_A$, where M_A is a trivalent or tetravalent metal ion and M_B is a divalent metal ion, e.g., Mn(II), have been synthesized by using the dimetal(II) anionic cores, $[(M^{II}_B)_2(dfmp)_3]^{5-}$ as a bridging ligand for the terminal LM_A fragments where H_3dfmp is a dinucleating phenol-oxime ligand, 2,6-diformyl-4-methylphenol oxime, and L denotes a facially coordinating cyclic tridentate amine, 1,4,7-trimethyl-1,4,7-triazacyclononane. The following combinations are reported here, $B^{III}Mn^{II}Mn^{II}B^{III}$ (**1**), $Mn^{III}Mn^{II}Mn^{II}Mn^{III}$ (**2**), $Mn^{IV}Mn^{II}Mn^{II}Mn^{IV}$ (**3**), $Fe^{III}Mn^{II}$-$Mn^{II}Fe^{III}$ (**4**), and $Cr^{III}Mn^{II}Mn^{II}Cr^{III}$ (**5**). The compounds have been characterized spectroscopically and by magnetic susceptibility measurements in the temperature range 2.0–290 K at different field strengths. Complexes **1**–**4** have also been structurally characterized by single-crystal X-ray diffraction techniques at 100 K. The magnetic behaviors of the compounds indicate weak antiferromagnetic coupling between the manganese(II) centers in the central trisphenoxo-bridged dimanganese(II) core, whereas the coupling between the terminal M_A and its neighboring Mn(II) center varies and is weak ferromagnetic or antiferromagnetic. The relative interaction intensity in such a series of complexes is discussed. Finally, a profound influence of the charge on the terminal metal ions on the strength of the exchange coupling in the central dimanganese(II) core has been observed and discussed in relation to the covalency of the metal–ligand bonding.

Introduction

Complexes containing two or more metal ions are of increasing interest because of their relevance to biological systems (as evidenced by the many multinuclear complexes in biology)[1] and to molecular magnetism.[2] Polynuclear systems are also ideal candidates for the synthesis of single-molecule magnets (SMMs).[3] Thus, the study of exchange interactions between paramagnetic metal centers through various bridging ligands has become an active research field in coordination chemistry with the aim of understanding fundamental factors governing the magnetic properties of transition metal compounds. Therefore, the interest in polynuclear complexes[4] of 3d transition metals has been augmented by the search for new magnetic clusters. Relatively few magnetic studies dealing with linear tetranuclear systems have been reported in contrast to the large number of studies dealing with tri- and dinuclear systems, primarily due to lack of fully structurally characterized compounds and to the increased complexity involved with the theoretical treatments of multispin systems. Despite the interest in the properties of such systems, synthetic methods have yet to reach the level of efficiency attained with mononuclear complexes.

Of particular concern in this context is the development of directed routes to specific complexes, particularly those in which the metals are connected by "robust" ligands so

* To whom correspondence should be addressed. E-mail: Chaudh@mpi-muelheim.mpg.de.

(1) Messerschmidt, A.; Huber R.; Poulos, T.; Wieghardt, K. Eds. *Handbook of Metalloproteins*; John Wiley and Sons: Chichester, U.K., 2001.

(2) Kahn, O. *Molecular Magnetism*; VCH: New York, 1993.

(3) Christou, G.; Gatteschi, D.; Hendrickson, D. N.; Sessoli, R. *MRS Bull.* **2000**, 66−71.

(4) For example, Winpenny, R. E. P. *Adv. Inorg. Chem.* **2001**, *52*, 1−111.

10.1021/ic060409a CCC: $33.50
Published on Web 06/24/2006

that fragmentation of the complexes in their subsequent reactions is inhibited. One particularly successful route involves the use of "metalloligands",[5] in which the ligands already bound to one metal have free coordination sites that can bind a second metal of the same or different kind. We have favored the strategy of "metal oximate" building blocks[6] as ligands to design and synthesize multinuclear complexes in a controlled fashion. This approach of using metalloligands containing polynucleating ligands proceeds step by step and provides a route to gain control of the nuclearity in addition to the preparation of species containing different metal ions, i.e., heterometallic complexes. Thus, in recent years we reported[7] series of homo- and heterometal complexes containing two, three, or four metal centers of the type M_AM_B, $M_AM_BM_A$, $(M_A)_2(\mu_3\text{-}O)_2(M_B)_2$, and $M_AM_BM_C$ utilizing metal oximates as ligands; these materials are unique and have been proved to be ideal for the investigations of exchange mechanism.

As an extension of the strategy of using "metal complexes" as bridging groups, we envisaged the possibility of preparing a series of linear tetranuclear complexes of the type $M_AM_B\text{-}M_BM_A$,[8] in which the central metal ions, M_B's, are embedded in a dinucleating phenol-oxime ligand, H_3dfmp (2,6-diformyl-4-methylphenol oxime). In this work, a dimanganese(II) building block, $[Mn^{II}_2(dfmp)_3]^{5-}$, is used as a bridging ligand and depicted below

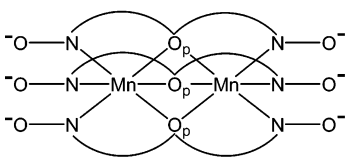

$[Mn^{II}_2(dfmp)_3]^{5-}$

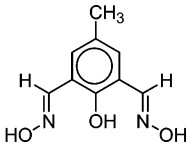

H_3dfmp

where $^-O{-}N{\cap}O_p{\cap}N{-}O^-$ represents the deprotonated oxime ligand, $dfmp^{3-}$.

Thus, tetranuclear complexes $M_AMn^{II}Mn^{II}M_A$ were easily achieved by using the capping (terminal) LM_A fragments (M_A = Mn^{IV}, Mn^{III}, Fe^{III}, or Cr^{III}), where L denotes a facially coordinating cyclic tridentate amine 1,4,7-trimethyl-1,4,7-triazacyclononane. The ability of the pentaanion, tris(2,6-diformyl-4-methylphenoldioximato)dimanganese(II), $[Mn^{II}_2(dfmp)_3]^{5-}$ to provide synthetic routes of assembling molecules with four magnetic subunits connected by bridging oximate groups, which ensures spin communication[6] within a single molecular entity, is reported here. There have been relatively few reports dealing with the coordination chemistry of 2,6-diformyl-4-methylphenol dioxime.[9] We described earlier[8] the synthesis of a tetranuclear complex, $Fe^{III}Ni^{II}Ni^{II}\text{-}Fe^{III}$, which was accomplished by using $Ni^{II}_2(Hdfmp)_2$ as a bridging ligand for the terminal Fe(III) centers.

We report herein deliberate synthesis and characterization of

$$[LMn^{III}\{\mu\text{-}(dfmp)_3Mn^{II}_2\}Mn^{III}L]ClO_4 \quad \mathbf{2}$$

$$[LMn^{IV}\{\mu\text{-}(dfmp)_3Mn^{II}_2\}Mn^{IV}L](ClO_4)_3 \quad \mathbf{3}$$

$$[LFe^{III}\{\mu\text{-}(dfmp)_3Mn^{II}_2\}Fe^{III}L]ClO_4 \quad \mathbf{4}$$

$$[LCr^{III}\{\mu\text{-}(dfmp)_3Mn^{II}_2\}Cr^{III}L]ClO_4 \quad \mathbf{5}$$

for magnetochemical studies. Moreover, as we want to explore the effect of terminal (capping) paramagnetic metal fragment, LM_A, on the exchange coupling of the central tris(phenolato)-bridged dimanganese(II) unit, we also synthesized a diamagnetic B(III)-capped, i.e., a dinuclear manganese(II), complex from the magnetic standpoint,

$$Et_3NH[(CH_3)B^{III}\{\mu\text{-}(dfmp)_3Mn^{II}_2\}B^{III}(CH_3)] \quad \mathbf{1}$$

Thus, complex **1** contains the identical dimetallic manganese(II) core as in **2**−**5**, but the terminal diamagnetic $(CH_3)\text{-}B^{III}$ fragment in **1**, originating from methylboronic acid $CH_3B(OH)_2$, has been replaced by the corresponding paramagnetic LMn^{III} **2**, LMn^{IV} **3**, LFe^{III} **4**, or LCr^{III} **5** fragments.

For the sake of clarity, the aforementioned complexes are denoted only by the metal centers throughout this paper.

Experimental Section

Physical Measurements. Fourier transform infrared spectroscopy on KBr pellets was performed on a Perkin-Elmer 2000 FT-IR instrument. Square wave and cyclic voltammetric experiments were performed with a EG&G potentiostat−galvanostat model 273 A at ambient temperature. A standard three-electrode cell was employed with a glassy-carbon working electrode, a silber-wire auxiliary electrode, and a Ag/AgCl (saturated LiCl in ethanol) reference electrode. The supporting electrolyte was 0.1 M $^nBu_4NPF_6$. Measurements were made under an argon atmosphere in dry solvents, viz. CH_3CN, CH_2Cl_2. The potential of the reference electrode was determined by utilizing ferrocenium(1+)/ferrocene

(5) (a) Gruber, S. J.; Harris, C. M.; Sinn, E. *J. Inorg. Nucl. Chem.* **1968**, *30*, 1805−1830. (b) Selbin, J.; Ganguly, L. *J. Inorg. Nucl. Chem. Lett.* **1969**, *5*, 815−818. (c) Linkvedt, R. L.; Kramer, L. S.; Ranger, G.; Corfield, P. W.; Glick, M. D. *Inorg. Chem.* **1983**, *22*, 3580−3587. (d) Singh, C. B.; Sahoo, B. *J. Inorg. Nucl. Chem.* **1974**, *36*, 1259−1264. (e) Luneau, D.; Oshio, H.; Okawa, H.; Kida, S. *J. Chem. Soc., Dalton Trans.* **1990**, 2283−2286. (f) Pal, S.; Mukherjee, R.; Tomas, M.; Falvello, L. R.; Chakravorty, A. *Inorg. Chem.* **1986**, *25*, 200−207. (g) Chaudhuri, P.; Winter, M.; Fleischhauer, P.; Haase, W.; Flörke, U.; Haupt, H.-J. *J. Chem. Soc., Chem. Commun.* **1990**, 1728−1730.

(6) (a) Chaudhuri, P. *Coord. Chem. Rev.* **2003**, *343*, 143−190. (b) Chaudhuri, P. *Proc. Indian Acad. Sci.* **1999**, *111*, 397−411.

(7) For example: (a) Burdinski, D.; Birkelbach, F.; Gerdan, M.; Trautwein, A. X.; Wieghardt, K.; Chaudhuri, P. *J. Chem. Soc., Chem. Commun.* **1995**, 963−964. (b) Birkelbach, F.; Winter, M.; Flörke, U.; Haupt, H.-J.; Butzlaff, C.; Lengen, M.; Bill, E.; Trautwein, A. X.; Wieghardt, K.; Chaudhuri, P. *Inorg. Chem.* **1994**, *33*, 3990−4001. (c) Chaudhuri, P.; Winter, M.; Della Vedova, B. P. C.; Bill, E.; Trautwein, A. X.; Gehring, S.; Fleischhauer, P.; Nuber, B.; Weiss, J. *Inorg. Chem.* **1991**, *30*, 2148−2157. (d) Birkelbach, F.; Flörke, U.; Haupt, H.-J.; Butzlaff, C.; Trautwein, A. X.; Wieghardt, K.; Chaudhuri, P. *Inorg. Chem.* **1998**, *37*, 2000−2008. (e) Chaudhuri, P.; Birkelbach, F.; Winter, M.; Staemmler, V.; Fleischhauer, P.; Haase, W.; Flörke, U.; Haupt, H.-J. *J. Chem. Soc., Dalton Trans.* **1994**, 2313−2319. (f) Verani, C. N.; Rentschler, E.; Weyhermüller, T.; Bill, E.; Chaudhuri, P. *J. Chem. Soc., Dalton Trans.* **2000**, 4263−4271 and references in the papers (a)−(f).

(8) Krebs, C.; Winter, M.; Weyhermüller, T.; Bill, E.; Wieghardt, K.; Chaudhuri, P. *J. Chem. Soc., Chem. Commun.* **1995**, 1913−1915.

(9) (a) Black, D.; Blake, A. J.; Dancey, K. P.; Harrison, A.; McPartlin, M.; Parsons, S.; Tasker, P. A.; Whittacker, G.; Schröder, M. *J. Chem. Soc., Dalton Trans.* **1998**, 3953−3960. (b) Okawa, H.; Tokii, T.; Muto, Y.; Kida, S. *Bull. Chem. Soc. Jpn.* **1973**, *46*, 2464−2467.

as the internal standard, and all potentials are quoted versus the Fc^+/Fc couple.

Magnetic susceptibilities of powdered samples were recorded on a SQUID magnetometer (MPMS, Quantum Design) in the temperature range 2−290 K with an applied field of 1 T. Experimental susceptibility data were corrected for the underlying diamagnetism using Pascal's constants. Mössbauer spectra were recorded on alternating constant-acceleration spectrometers. The minimum experimental line width was 0.24 mm s^{-1} full width at half-maximum. The sample temperature was kept constant either in an Oxford Variox or an Oxford Mössbauer-Spectromag cryostat. With the help of re-entrant bore tubes, the $^{57}Co/Rh$ source was positioned at room-temperature inside the gap of the magnet system at a distance of about 85 mm from the sample. The field is zero at this position. Isomer shifts are given relative to α-Fe at room temperature.

Chemicals. The macrocycle 1,4,7-trimethyl-1,4,7-triazacyclononane (L = $C_9H_{21}N_3$) and its iron complex $LFeCl_3$ were prepared as described previously.[10] All other starting materials were commercially available and mostly of reagent grade. Elemental analyses (C, H, N) were performed by Microanalytical Laboratory Dornis and Kolbe, Mülheim a.d. Ruhr.

2,6-Diformyl-4-methylphenol was synthesized as described in ref 11. The corresponding dioxime, H_3dfmp, was prepared in the following way: To a suspension of 2,6-diformyl-4-methylphenol (3.36 g; 20 mmol) and $NH_2OH{\cdot}HCl$ (3.13 g; 45 mmol) in water (50 mL), warmed at 80 °C, was added methanol with stirring until a clear orange solution was obtained. The solution was stirred at 80 °C for 1 h. The solution was cooled to room temperature followed by addition of enough water so that the solution just started to become turbid. After the mixture was kept at ambient temperature for ca. 24 h, the crystalline solid was removed by suction filtration, washed thoroughly with water, and dried in air. The dioxime can be recrystallized from a methanol−water mixture. Yield: 4.5 g (70%). mp 186−188 °C. IR (KBr, medium and strong selective bands only): 3380, 3329, 1623, 1604, 1465, 1307, 1265, 1061, 1027, 934, 793, 757, 696 cm^{-1}. ^1H NMR (CD_3OD, 80 MHz): δ 2.34 (3H, s, CH_3), 7.37 (2H, s, Ar), 8.37 (2H, s, oxime). ^{13}C NMR ($CDCl_3$): δ 20.31 ($ArCH_3$), 119.78, 129.84, 130.85 (C−Ring), 149.17 (CN), 154.48 (C−OH). EI-MS: *m*/*z* 194 (M^+, 100%).

Preparation of Complexes. $Et_3NH[(CH_3)B^{III}\{\mu\text{-}(dfmp)_3Mn^{II}_2\}B^{III}(CH_3)]$ (1). To a solution of H_3dfmp (300 mg, 1.5 mmol) and $Mn(ClO_4)_2{\cdot}6H_2O$ (370 mg, 1 mmol) in methanol (40 mL) was added triethylamine (0.6 mL, 4.5 mmol), and the suspension was stirred for 10 min. To this dark solution methylboronic acid $CH_3B(OH)_2$ (60 mg, 1 mmol) was added. The solution was stirred at ambient temperature for 0.5 h in air, after which the precipitated deep yellow solid was collected by filtration and air-dried. The yellow solid was recrystallized from a solvent mixture of dichloromethane−ethanol (2:1). Yield: 290 mg (40%). Anal. Calcd for $C_{35}H_{43}N_7O_9B_2Mn_2$: C, 50.18; H, 5.14; N, 11.7; Mn, 13.15. Found: C, 49.8; H, 4.85; N, 11.56; Mn, 13.19. IR(KBr, cm^{-1}): 1610, 1593, 1580, 1450, 1305, 1208, 1047, 1008, 946, 935, 833, 761, 738, 705. ESI-MS (negative ion) (*m*/*z*): 735.2 (100%) [M − $Et_3NH]^-$; ESI-MS (positive): 102.2 (100%) (Et_3NH^+).

$[LMn^{III}\{(dfmp)_3Mn^{II}_2\}Mn^{III}L](ClO_4)$ (2). Under argon, 300 mg (1.5 mmol) of H_3dfmp was dissolved in 30 mL of methanol, and 0.4 mL (3 mmol) of triethylamine was added and stirred for 10 min. Then, 0.24 g (1 mmol) of $Mn^{II}(CH_3COO)_2{\cdot}4H_2O$ was added and stirred. In another round-bottomed flask, 0.17 g (1 mmol) of 1,4,7-trimethyl-1,4,7-triazacyclononane (L) and 0.26 g of $[Mn^{III}_3(\mu\text{-}O)(\mu\text{-}CH_3COO)_6(H_2O)_3](CH_3COO)$ dissolved in 20 mL of methanol were stirred for 20 min. This solution was added to the previous solution and was refluxed for 20 min when the resulting solution turned brown-black. After cooling, the solution was filtered and 0.24 g (2 mmol) of $NaClO_4$ was added to brown precipitate, which was collected by filtration and air-dried. Suitable single crystals for X-ray analysis were grown from an acetonitrile−methanol (3:1) mixture. Yield: 400 mg (37%). Anal. Calcd for $C_{45}H_{63}N_{12}O_9(ClO_4)Mn_4$: C, 43.75; H, 5.14; N, 13.62; Mn, 16.84. Found: C, 43.93; H, 5.2; N, 13.81; Mn, 16.64. IR(KBr, cm^{-1}): 2918, 1608, 1567, 1542, 1438, 1322, 1229, 1120, 1108, 1079, 1003, 988, 720, 624. ESI-MS (positive) in CH_3CN: (*m*/*z*): 567.8 (73%) [**2** − ClO_4 + $H^+]^+$, 1135.2 (100%) [**2** − $ClO_4]^+$, 1234.3 (10%) [**2** + $H]^+$.

$[LMn^{IV}\{(dfmp)_3Mn^{II}_2\}Mn^{IV}L](ClO_4)_3$ (3). In a flask 0.17 g (1 mmol) of 1,4,7-trimethyl-1,4,7-triazacyclononane and 0.26 g of $[Mn^{III}_3(\mu\text{-}O)(\mu\text{-}CH_3COO)_6(H_2O)_3](CH_3COO)$ were dissolved in 20 mL of methanol and were stirred for 20 min. This solution was added to the assembled dimanganese(II) unit, as described for **2**, and refluxed for 20 min in air when the resulting solution turned brown-black. After cooling, the solution was filtered and 0.24 g (2 mmol) of $NaClO_4$ was added, and the precipitated brown solid was collected by filtration and air-dried. Suitable single crystals of X-ray quality were grown from acetonitrile−ethanol (3:1). Yield: 300 mg (29%). Anal. Calcd for $C_{45}H_{63}N_{12}O_9(Cl_3O_{12})Mn_4$: C, 37.69; H, 4.43; N, 11.72; Mn, 15.32. Found: C, 37.4; H, 4.8; N, 11.7; Mn, 14.62. IR(KBr, cm^{-1}): 2919, 1608, 1567, 1541, 1436, 1322, 1230, 1090, 1001, 984, 819, 722, 624. ESI-MS (positive) in CH_3CN: (*m*/*z*), 567.7 (100%), 1135.4 (90%), 1234.3 (10%).

$[LFe^{III}\{(dfmp)_3Mn^{II}_2\}Fe^{III}L](ClO_4)$ (4). H_3dfmp (300 mg, 1.5 mmol) was dissolved in 30 mL of methanol, and 0.5 mL (4 mmol) of triethylamine was added to it and was stirred for 10 min. Then, 0.24 g (1 mmol) of $Mn^{II}(CH_3COO)_2{\cdot}4H_2O$ was added and stirred followed by $LFeCl_3$ (0.33 g, 1 mmol), then the mixture was refluxed for 20 min under argon, and the resulting solution turned brown-black. After cooling, the solution was filtered and 0.24 g (2 mmol) of $NaClO_4$ was added and, after a few minutes, a red-brown solid precipitated and it was filtered through suction filtration, washed with diethyl ether, and then dried in air. Suitable single crystals for X-ray diffraction were grown from acetonitrile−dichloromethane (1:3). Yield: 390 mg (36%). Anal. Calcd for $C_{45}H_{63}N_{12}O_9(ClO_4)Fe_2Mn_2$: C, 43.69; H, 5.13; N, 13.59; Mn, 8.88; Fe, 9.03. Found: C, 43.2; H, 4.95; N, 13.57; Mn, 8.21 Fe, 8.8. IR(KBr, cm^{-1}): 2922, 1608, 1576, 1434, 1315, 1229,1121, 1087, 1005, 988, 816, 717, 624. ESI-MS (positive) (*m*/*z*):, 1137.2(100%) [**4** − $ClO_4]^+$.

$[LCr^{III}\{(dfmp)_3Mn^{II}_2\}Cr^{III}L](ClO_4)$ (5). To a suspension of 0.46 g (1 mmol) of $L{\cdot}CrBr_3$ in 30 mL of methanol was slowly added 0.42 g (2 mmol) of $AgClO_4$ with stirring. The suspension was refluxed under argon for 0.5 h; during this time, a blue-violet solution with a concomitant formation of AgBr resulted. Precipitated AgBr was filtered off, and the clear blue-violet solution was added to the previously described (see complex **2**) methanolic solution of the dimanganese units. The mixed solutions were refluxed for 20 min under argon when the resulting solution turned brown-black. After cooling, the solution was filtered to give a green-brown microcrystalline solid, which was washed with diethyl ether and then dried in air. Yield: 390 mg (36%). Anal. Calcd for $C_{45}H_{63}N_{12}O_{13}ClMn_2Cr_2$: C, 43.96; H, 5.17; N, 13.67; Mn, 8.94; Cr, 8.46. Found: C, 43.4; H, 5.14; N, 13.6; Mn, 8.71; Cr, 8.59. IR(KBr, cm^{-1}): 1607, 1579, 1560, 1460, 1444, 1305, 1226, 1031, 1006, 988, 705. ESI-MS (positive) (*m*/*z*): 1129.3 (100%) [**5** − $ClO_4]^+$.

(10) Chaudhuri, P.; Winter, M.; Wieghardt, K.; Gehring, S.; Haase, W.; Nuber, B.; Weiss, J. *Inorg. Chem.* **1988**, *27*, 1564−1569.
(11) Verani, C. N.; Rentschler, E.; Weyhermüller, T.; Bill, E.; Chaudhuri, P. *J. Chem. Soc., Dalton Trans.* **2000**, 251−258.

Table 1. Crystallographic Data and Structure Refinement for **1**, **2**, **3**, and **4**

	1·C_2H_5OH	**2**·CH_3CN·CH_3OH	**3**·0.5CH_3CN·1.5H_2O	**4**·0.5CH_2Cl_2·CH_3CN
empirical formula	$C_{37}H_{49}B_2N_7O_{10}Mn_2$	$C_{48}H_{70}ClN_{13}O_{14}Mn_4$	$C_{46}H_{67.5}Cl_3N_{12.5}O_{22}Mn_4$	$C_{47.5}H_{67}Cl_2N_{13}O_{13}Mn_2Fe_2$
fw	883.33	1308.38	1481.73	1320.62
temp	100(2) K	100(2) K	100(2) K	100(2) K
wavelength (Mo Kα)	0.71073 Å	0.71073 Å	0.71073 Å	0.71073 Å
cryst syst	trigonal	monoclinic	triclinic	monoclinic
space group	$P3_121$	$P2(1)/c$	$P\bar{1}$	$P2(1)/c$
unit cell dimens	$a = 11.2698(3)$ Å	$a = 16.485(2)$ Å	$a = 17.0262(4)$ Å	$a = 14.4112(4)$ Å
	$b = 11.2698(3)$ Å	$b = 14.494(2)$ Å	$b = 18.2672(4)$ Å	$b = 16.6991(6)$ Å
	$c = 27.7328(7)$ Å	$c = 24.365(3)$ Å	$c = 23.5979(6)$ Å	$c = 25.0197(8)$ Å
	$\alpha = 90°$	$\alpha = 90°$	$\alpha = 101.44\ (1)°$	$\alpha = 90°$
	$\beta = 90°$	$\beta = 90.26(2)°$	$\beta = 108.57(1)°$	$\beta = 104.82(4)°$
	$\gamma = 120°$	$\gamma = 90°$	$\gamma = 105.65(1)°$	$\gamma = 90°$
vol (Å^3); Z	3050.4(14); 3	5821.6(13); 4	6366.2; 4	5820.8(3); 4
density (calcd) Mg/m^3	1.443	1.493	1.546	1.507
absorp. coeff. (mm^{-1})	0.686	0.966	0.984	1.075
F(000)	1380	2712	3048	2732
cryst size (mm^3)	0.18 × 0.17 × 0.12	0.11 × 0.06 × 0.02	0.12 × 0.10 × 0.05	0.06 × 0.05 × 0.05
θ range for data collect.	3.04−30.48°	3.18−22.50°	2.92−27.5°	2.08−30.55°
reflns collected	63 879	49 350	114 428	65 527
independent reflns	6165 [R(int) = 0.0424]	7587 [R(int) = 0.1495]	29 183 [R(int) = 0.0721]	17 765 [R(int) = 0.0631]
absorpt. correction	not corrected	not corrected	Gaussian, face indexed	not corrected
refinement method	full-matrix least-squares on F^2	full-matrix least-squares on F^2	full-matrix least-squares on F^2	full-matrix least-squares on F^2
data/restraints/params	6157/9/281	7587/8/711	29 183/906/1655	17 632/7/760
GOF on F^2	1.107	1.216	1.029	1.012
final R indices	R1 = 0.0379	R1 = 0.1044	R1 = 0.0756	R1 = 0.0527
[$I > 2\sigma(I)$]	wR2 = 0.0980	wR2 = 0.1595	wR2 = 0.1929	wR2 = 0.1263
R indices (all data)	R1 = 0.0420	R1 = 0.1430	R1 = 0.1075	R1 = 0.0856
	wR2 = 0.1130	wR2 = 0.1737	wR2 = 0.2143	wR2 = 0.1494
largest diff. peak and hole, eÅ^{-3}	0.621/−0.303	0.656/−0.504	3.036/−1.063	1.583/−1.087
absolute structure param	0.02(2)	−	−	−

CAUTION: Although we experienced no difficulties with the compounds isolated as their perchlorate salts, the unpredictable behavior of perchlorate salts necessitates extreme caution in their handling!

X-ray Crystal Structure Determinations. The crystallographic data for **1**−**4** are summarized in Table 1. Graphite-monochromated Mo Kα radiation(λ = 0.71073 Å) was used for **1**−**4**. Dark red-brown red crystals of **1**−**4** were fixed with perfluoropolyether onto glass fibers and mounted on a Bruker-Nonius Kappa CCD diffractometer equipped with a cryogenic nitrogen cold stream, and intensity data were collected at 100(2) K. Final cell constants were obtained from a least-squares fits of all integrated reflections. Intensity data were corrected for Lorentz and polarization effects The data set for **1**, **2**, and **4** was not corrected for absorption. The data set for **3** was corrected for absorption using the Gaussian-type absorption correction routine embedded in XPREP. The Siemens ShelXTL software package was used for solution refinement[12] and artwork of the structures; the neutral atom scattering factors of the program were used.

Results and Discussion

A straightforward, moderate-yield modular synthetic route to pure linear tetranuclear, both homo- and heteronuclear, complexes containing tris-phenolato and consequently tris-oximato bridges has been developed as outlined in Scheme 1.

The reactions are clean, affording pure crystalline product in moderate yield (30−40%). The thermodynamic stability of the terminal metal ions (Cr^{III}, Mn^{III}, Mn^{IV}, and Fe^{III}) with the macrocyclic tridentate amine ligand L[13] and the stabilization of the lower redox state (+II) for the central metal ions (Mn^{II}) by the enforced trigonal distortion (twist angles 0.8−12.8°) through the present rigid N_3O_3-donor sets[14] are utilized to synthesize tetranuclear $M_AM_BM_BM_A$ complexes.

It is noteworthy that, in contrast to modular synthesis for heterometal complexes, it was not necessary to isolate the intermediates for this synthetic route. The colors of the tetranuclear complexes are yellow for **1** and light-to-deep-red/brown for **2**−**5**. They are air-stable in the solid state and also in solution for a few days, except for **2**.

Since the relevant bands in the IR spectra of comparable oxime-containing homo- and heterometal complexes have been described earlier[7,15] and the spectra of complexes **1**−**5** are also very similar, we refrain from discussing them in detail. The bands are given in the Experimental Section.

Electrospray-ionization mass spectrometry (ESI-MS) in the negative-ion mode proved to be very useful analytical tool for characterizing complex **1**, which shows the mononegatively charged species [**1** − Et_3NH]$^-$ as the base peak at m/z 735.2. As expected, the monopositive cation Et_3NH^+ in **1** is shown at m/z 102.2. On the other hand, the ESI-MS

(12) (a) Sheldrick, G. M. *SHELXTL*, Ver. 5; Siemens Analytical X-ray Instruments, Inc.: Malvern, PA, 1994. (b) Sheldrick, G. M. *SHELXL-97*; University of Göttingen: Göttingen, Germany, 1997.

(13) Chaudhuri, P.; Wieghardt, K. *Prog. Inorg. Chem.* **1987**, *35*, 329−436.

(14) (a) Drew, M. G. B.; Harding, C. J.; McKee, V.; Morgan, G. G.; Nelson, J. *J. Chem. Soc., Chem. Commun.* **1995**, 1035−1038. (b) Chakravorty, P.; Chandra, S. K. *Polyhedron* **1994**, *13*, 683−687.

(15) (a) Burdinski, D.; Birkelbach, F.; Weyhermüller, T.; Flörke, U.; Haupt, H.-J.; Lengen, M.; Trautwein, A. X.; Bill, E.; Wieghardt, K.; Chaudhuri, P. *Inorg. Chem.* **1998**, *37*, 1009−1020. (b) Birkelbach, F.; Weyhermüller, T.; Lengen, M.; Gerdan, M.; Trautwein, A. X.; Wieghardt, K.; Chaudhuri, P. *J. Chem. Soc., Dalton Trans.* **1997**, 4529−4537. (c) Ross, S.; Weyhermüller, T.; Bill, E.; Wieghardt, K.; Chaudhuri, P. *Inorg. Chem.* **2001**, 40, 6656−6665. (d) Ross, S.; Weyhermüller, T.; Bill, E.; Bothe, E.; Flörke, U.; Wieghardt, K.; Chaudhuri, P. *Eur. J. Inorg. Chem.* **2004**, 984−997.

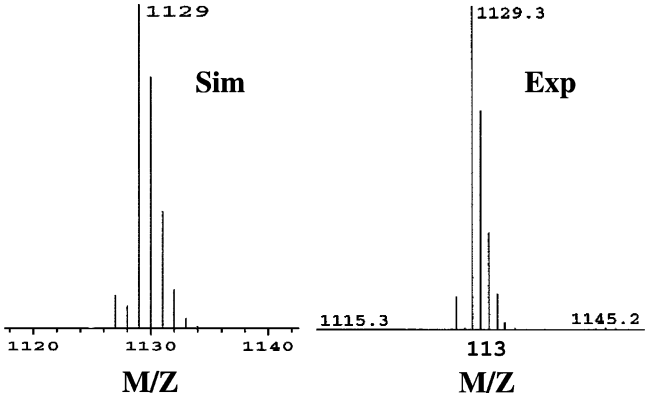

Figure 1. Positive-ion ESI mass spectrum of complex **5**, $Cr^{III}Mn^{II}Mn^{II}Cr^{III}$, with calculated (sim) and experimental isotopic distributions for the base peak $(\mathbf{5} - ClO_4)^+$.

results in the positive-ion mode were successful in characterizing **2**−**5** and were very similar. There is practically no indication in the spectra for ligand fragmentation or cleavage of the central Mn(II) dimer, which indicates the robustness of the clathrochelates, i.e., multicyclic ligand systems that completely encapsulate a metal ion, derived from the 2,6-diformyl-4-methylphenoldioxime. Complexes **1**−**5** are not fragile and can withstand the conditions of ESI-MS ionization. The mass spectra of complexes **2** and **3** exhibit identical ions (albeit with different intensities, see Experimental Section), although they contain the terminal manganese ions in different oxidation states; complex **3** containing Mn(IV) undergoes a fast redox reaction prior to forming ions in the gas phase to produce complex **2** with Mn(III) ions and hence gives mass spectrum as that of **2**. Shown in Figure 1 is the positive-ion ESI mass spectrum of **5**, $Cr^{III}Mn^{II}Mn^{II}Cr^{III}$, together with the calculated isotope pattern for the base peak $[\mathbf{5} - ClO_4]^+$.

Electrochemistry. Cyclic voltammograms of complexes **1** and **2** were recorded in CH_3CN containing 0.1 M $^nBu_4NPF_6$ in the potential range −2.25 to +1.25 V vs Fc^+/Fc. The CV of **1** afforded one $2e^-$ reversible oxidation processes at ca. 0.55 V vs Fc^+/Fc, which is shown in Figure 2. The oxidation is central manganese centered and represents the Mn^{II}/Mn^{III} couple for both Mn(II) ions.

The CV of complex **2** (Figure 2) exhibits two consecutive $2e^-$ oxidation processes in the potential range from 0.00 to 1.0 V vs Fc^+/Fc and one $2e^-$ reduction at −0.75 V vs Fc^+/Fc. The first pair of oxidations is assigned to the oxidation of two terminal Mn(III) centers to their Mn(IV) forms; aerial oxidation of complex **2** containing terminal Mn(III) ions to complex **3** with terminal Mn(IV) ions is in full accord with the electrochemical assignment. The very similar oxidation potential for the $Mn^{III}Mn^{IV}$ couples indicates negligible interactions between the terminal manganese centers. The second pair of oxidations then clearly belongs to the central manganese ions, and the comparatively high oxidation potentials for the couple Mn^{II}/Mn^{III} reflects that in aerobic conditions the oxidation of central Mn(II) is highly unfavorable. Therefore, the oxidation equilibria are expressed as follows

$$Mn^{III}Mn^{II}Mn^{II}Mn^{III} \overset{ox_1}{\rightleftharpoons} Mn^{IV}Mn^{II}Mn^{II}Mn^{IV} \overset{ox_2}{\rightleftharpoons} Mn^{IV}Mn^{III}Mn^{III}Mn^{IV}$$

The $2e^-$ reduction step in the more negative potential (−0.75 V vs Fc^+/Fc) is attributable to the following equilibrium

$$Mn^{III}Mn^{II}Mn^{II}Mn^{III} \overset{red_1}{\rightleftharpoons} Mn^{II}Mn^{II}Mn^{II}Mn^{II}$$

The comproportionation constant, K_c, for the equilibrium

$$Mn^{III}Mn^{II}Mn^{II}Mn^{III} + Mn^{IV}Mn^{II}Mn^{II}Mn^{IV} \overset{K_C}{\rightleftharpoons} 2\ Mn^{IV}Mn^{II}Mn^{II}Mn^{III}$$

is calculated to be only 22, showing that the isolation of the

Scheme 1

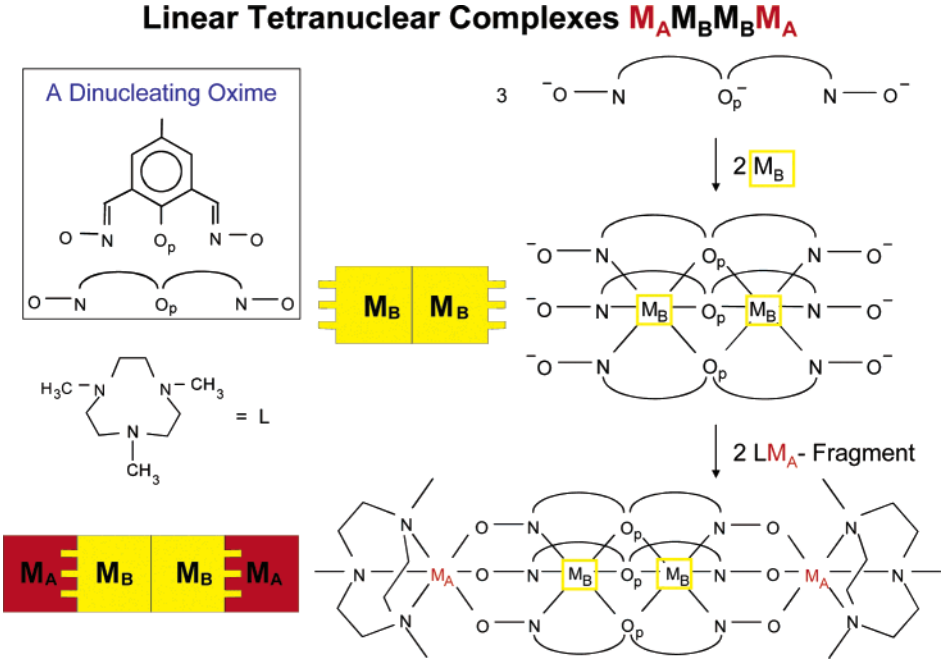

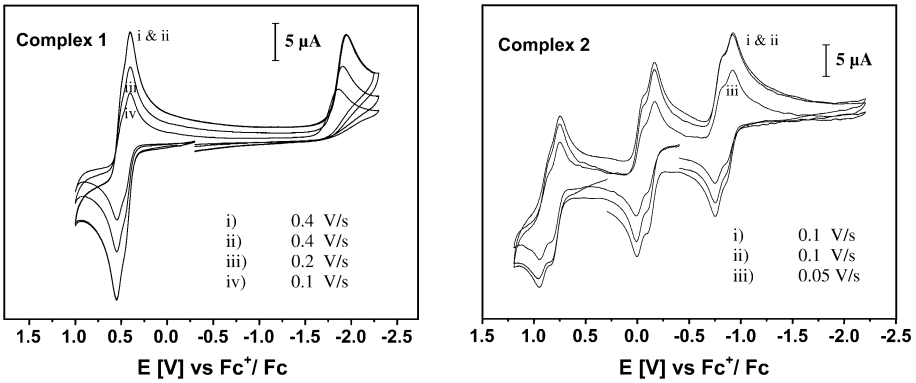

Figure 2. Cyclic voltammograms at ambient temperature for complexes **1** and **2** in CH_3CN at different scan rates.

mixed-valence species $Mn^{IV}Mn^{II}Mn^{II}Mn^{III}$ is very unfavorable. Accordingly, all our attempts to isolate the species failed.

Mössbauer Parameters for 4. The Mössbauer spectrum for **4** was measured at 80 K in zero field to determine the spin and oxidation state of the iron centers. Mössbauer results indicate a single quadrupole splitting in accordance with only one type of iron coordination sphere in the solid-state structure, namely the iron site coordinated to the cyclic amine 1,4,7-trimethyl-1,4,7-triazacyclononane, L. An isomer shift of $\delta_{Fe} = 0.48$ mm s^{-1} and a quadrupole splitting of $\Delta E_Q = 0.42$ mm s^{-1} for **4** are consistent with those observed[15d,16] for d^5 high-spin electron configuration for the iron centers with FeN_3O_3 coordination environments. This assignment is also confirmed by the X-ray structure of **4**.

Description of the Structures. Molecular Structure of $[(CH_3B)_2Mn^{II}_2(dfmp)_3]Et_3NH\cdot C_2H_5OH$ ($1\cdot C_2H_5OH$). The lattice consists of discrete tetranuclear monoanions containing the $B^{III}Mn^{II}Mn^{II}B^{III}$ unit, triethylammonium cations, and ethanol molecules of crystallization. Figure 3 displays the structure of the monoanion in **1**. The X-ray structure confirms that a linear tetranuclear complex has indeed been formed in such a way that each manganese center with a MnN_3O_3 donor set is embedded in a clathrochelate derived from the 2,6-diformyl-4-methylphenoldioximate ligand. The central tris(oximato)bismanganese(II), $[Mn_2(dfmp)_3]^{5-}$, bridges two terminal $(CH_3)B^{III}$ centers through the deprotonated oximate oxygen atoms. All phenoxy oxygen atoms, O38, O23, and O23*, are μ_2-bridging, yielding a Mn(1)···Mn(1)* separation of 2.909 Å and a face-shared bioctahedral structure for the dimanganese(II) core. Selected bond lengths and angles are given in Table 2. The Mn−O and Mn−N bond lengths are in accord with a high-spin d^5 electron configuration.[17] That the central dimanganese bioctahedron is severely distorted is shown by the different Mn^{II}−O(Phenoxo) bond lengths: Mn1−O38 = 2.119(2) Å vs Mn1−O23 = 2.142(2) Å. This may be attributed to the rigidity of the clathrochelate formed. Such a tris(μ-phenoxo)dimanganese core is quite rare.[14b] The

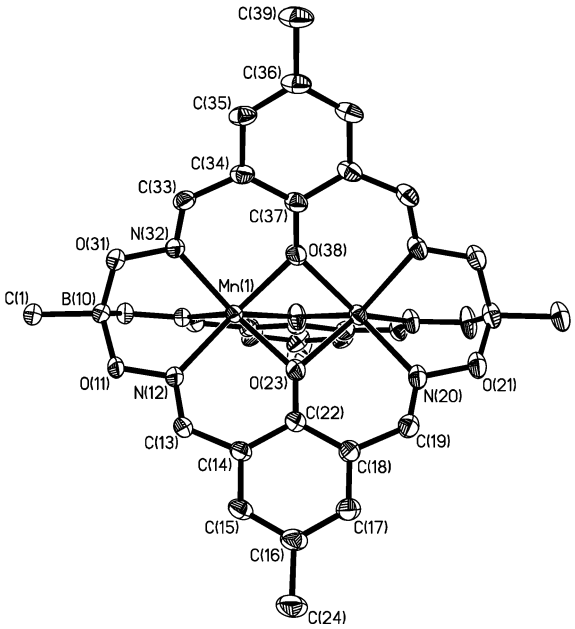

Figure 3. ORTEP representation of the anion in complex **1**, $B^{III}Mn^{II}$-$Mn^{II}B^{III}$.

coordination polyhedron around the manganese center is a trigonal prism with trigonal twist angles of 1.1°, 1.2°, and 0°. The average Mn1−N(oxime) distance, 2.174(2) Å, is shorter than those found in comparable high-spin Mn(II)−N(oxime)[7d,18] structures, 2.285(10) and 2.366(20) Å, but appreciably longer than those found in low-spin Mn(II)−N(oxime) structures, 1.95 Å.[19] The usual coordination number of Mn(II) is 6, and since high-spin Mn(II) obtains no ligand-field stabilization in either an octahedral or a tetrahedral environment, the geometry around the Mn(1) and Mn(1)* is dictated by the ligand constraints. In this case, we observe a six-coordinate complex with a trigonal prismatic geometry. The Mn1−O_{Phen}−Mn1* angles are in the range of 86.04−86.67°. Since the manganese-bridging oxygen bond distances, 2.119(2)−2.142(2) Å, are comparable to those found in the bis(phenoxo)-bridged[20] dimanganese complexes, the small Mn1−O_{Phen}−Mn1* angles force a comparatively short Mn···Mn separation of 2.909(5) Å.

(16) (a) Chaudhuri, P.; Rentschler, E.; Birkelbach, F.; Krebs, C.; Bill, E.; Weyhermüller, T.; Flörke, U. *Eur. J. Inorg. Chem.* **2003**, 541−555. (b) Verani, C. N.; Bothe, E.; Burdinski, D.; Weyhermüller, T.; Flörke, U.; Chaudhuri, P. *Eur. J. Inorg. Chem.* **2001**, 2161−2169.

(17) *Comprehensive Coordination Chemistry*; Wilkinson, G., Ed.; Pergamon Press: Oxford, 1987.

(18) (a) Jurisson, S.; Francesconi, L.; Linder, K. E.; Treher, E.; Malley, M. F.; Gougoutas, J. Z.; Nunn, A. D. *Inorg. Chem.* **1991**, *30*, 1820−1827.

(19) Basu, P.; Chakravorty, A. *Inorg. Chem.* **1992**, *31*, 4980−4986.

Table 2. Selected Bond Lengths (Å) and Angles (deg) for $B^{III}Mn^{II}Mn^{II}B^{III}$, **1**[a]

Mn(1)−O(38)	2.119(2)	B(10)−O(31)	1.496(3)
Mn(1)−O(23)	2.142(2)	B(10)−O(21)#1	1.499(3)
Mn(1)−N(32)	2.173(2)	B(10)−O(11)	1.505(3)
Mn(1)−N(12)	2.174(2)	N(20)−Mn(1)#1	2.176(2)
C(1)−B(10)	1.610(3)	O(23)−Mn(1)#1	2.122(2)
O(38)−Mn(1)−O(23)#1	77.97(5)	O(23)−Mn(1)−N(12)	80.57(6)
O(38)−Mn(1)−O(23)	77.52(5)	N(32)−Mn(1)−N(12)	86.25(7)
O(23)#1−Mn(1)−O(23)	79.72(8)	O(38)−Mn(1)−N(20)#1	135.43(5)
O(38)−Mn(1)−N(32)	81.42(6)	O(23)#1−Mn(1)−N(20)#1	81.39(6)
O(23)#1−Mn(1)−N(32)	135.50(7)	O(23)−Mn(1)−N(20)#1	136.34(7)
O(23)−Mn(1)−N(32)	133.00(8)	Mn(1)#1−O(23)−Mn(1)	86.03(6)
O(38)−Mn(1)−N(12)	135.72(5)	Mn(1)#−O(38)−Mn(1)	86.68(8)
O(23)#1−Mn(1)−N(12)	134.63(7)		
N(32)−Mn(1)−N(20)#1	86.52(7)	O(31)−B(10)−C(1)	107.2(2)
N(12)−Mn(1)−N(20)#1	85.48(7)	O(21)#1−B(10)−C(1)	105.8(2)
O(31)−B(10)−O(21)#1	113.2(2)	O(11)−B(10)−C(1)	105.3(2)
O(31)−B(10)−O(11)	112.2(2)	Mn(1)···Mn(1)#1	2.9090(5)
O(21)#1−B(10)−O(11)	112.4(2)	B(10)···B(10)#1	8.664(2)

[a] Symmetry transformations used to generate equivalent atoms: #1, *y*, *x*, −*z*; #2, *x* − *y*, −*y*, −*z* − 1/3.

The terminal B(III) ions, B10 and B10*, are tetrahedrally coordinated with a carbon atom of the methyl group, C(1), and three oxygen atoms from the oximate groups, O11, O21*, and O31. The average B−O length is 1.500(5) Å. An intramolecular B···B separation of 8.864(2) Å has been found. Such B-capped clathrochelates are quite common in the literature,[21] particularly for the metal ions with low-spin d^6 electron configuration, but it is quite rare for high-spin Mn(II) centers.[18]

Molecular Structures of $[LMn^{III}\{\mu\text{-}(dfmp)_3Mn^{II}\}Mn^{III}L]ClO_4\cdot CH_3CN\cdot CH_3OH$ (2), $[LMn^{IV}\{\mu\text{-}(dfmp)_3Mn^{II}\}Mn^{IV}L](ClO_4)_3\cdot 0.5CH_3CN\cdot 1.5H_2O$ (3), and $[LFe^{III}\{\mu\text{-}(dfmp)_3\}Mn^{II}\}\text{-}Fe^{III}L]ClO_4\cdot 0.5CH_2Cl_2\cdot CH_3CN$ (4). The X-ray structures confirm that linear tetranuclear complexes M_A-$Mn^{II}Mn^{II}M_A$ (M_A = Mn(III), Mn(IV), or Fe(III)) have indeed been formed with a geometry in which two terminal pseudo-octahedral polyhedra are joined by three oximato N−O groups, derived from the central $[Mn^{II}_2(dfmp)_3]^{5-}$ core. The terminally coordinated macrocyclic ligand L exhibits no unexpected features.[13] The N−O (average 1.390 ± 0.01 Å) and C=N_{ox} (average 1.288 ± 0.005 Å) bond lengths and C−N_{ox}−O bond angles (average 111.8 ± 0.4°) of the bridging oximate ligands are found to be very similar to those of other comparable structures,[7−9] including those of **1** (1.399 ± 0.002 Å, 1.287 ± 0.004 Å, and 112.2 ± 0.2° for N−O, C=N_{ox}, and C−N_{ox}−O, respectively). As expected, the donor atoms for the metal ions of the cations in **2**−**4** are identical, $M_AN_3O_3$ for Mn^{III} (**2**), Mn^{IV} (**3**), Fe^{III} (**4**), and $Mn^{II}(O_{Phen})_3(N_{ox})_3$, but not the coordination geometry. Perspective views of the cations for **2**, **3**, and **4** are shown in Figure 4.

The coordination geometry of the terminal metal ions, viz. Mn(III) for **2**, Mn(IV) for **3**, and Fe(III) for **4**, is distorted octahedral with three nitrogen atoms, N(1), N(4), N(7) or N(21), N(24), N(27), from the facially coordinated tridentate macrocyclic amine L and three oxygen atoms, O(41), O(61), O(81) or O(51), O(71), O(91), from the bridging oximate groups (Figure 4). The bond lengths Mn(1)−N, Mn(4)−N (av ∼2.190 Å) and Mn(1)−O, Mn(4)−O (av ∼1.944 Å) for complex **2** correspond to the structures for high-spin d^4 electron-configured Mn(III) centers with very similar ligands.[6] The N−Mn(1)−N, N−Mn(4)−N angles fall between 79.0(3)° and 82.1(3)°, whereas the O−Mn(1)−O and O−Mn(4)−O angles vary from 97.1(3)° to 99.6(3)°. In summary, both structural parameters and charge-balance consideration for **2** unequivocally indicate +III oxidation states for the terminal manganese centers. An intramolecular Mn(1)···Mn(4) separation of 10.129 Å has been found. In contrast to **2**, the terminal Mn−O (average 1.848 ± 0.012 Å) and Mn−N (average 2.090 ± 0.006 Å) for **3** are significantly shorter, as expected for the terminal Mn(IV) centers and similar to those observed earlier[15b] in comparable structures with the cyclic amine. Additionally, absence of Jahn−Teller distortion and the tripositive nature of the cation are consistent with a d^3 electron configuration of the terminal Mn(IV) centers. The terminal Fe(III) ions, Fe(1) and Fe(2), in **4** are also in distorted octahedral geometry with the bond lengths Fe−N (average 2.231 ± 0.008 Å) and Fe−O (1.925 ± 0.016 Å),

(20) For example: (a) Kessissoglou, D. P.; Butler, W. M.; Percoraro, V. L. *Inorg. Chem.* **1987**, *26*, 495−503. (b) Chang, H.-R.; Larsen, S. C.; Boyd, P. D. W.; Pierpont, C. G.; Hendrickson, D. N. *J. Am. Chem. Soc.* **1988**, *110*, 4565−4576. (c) Yu, S.-B.; Wang, C.-P.; Day, E. P.; Holm, R. H. *Inorg. Chem.* **1991**, *30*, 4067−4074. (d) Higuchi, C.; Sakiyama, H.; Okawa, H.; Fenton, D. E. *J. Chem. Soc., Dalton Trans.* **1995**, 4015−4020. (e) Gallo, E.; Solari, E.; Re, N.; Floriani, C.; Chiesi-Villa, A.; Rizzoli, C. *J. Am. Chem. Soc.* **1997**, *119*, 5144−5154. (f) Blanchard, S.; Blondin, G.; Riviére, E.; Nierlich, M.; Girerd, J.-J. *Inorg. Chem.* **2003**, *42*, 4568−4578. (g) Hureau, C.; Anxolabéhère-Mallart, E.; Nierlich, M.; Gonnet, F.; Riviére, E.; Blondin, G. *Eur. J. Inorg. Chem.* **2002**, 2710−2719 and references therein. (h) Alexiou, M.; Dendrinou-Samara, C.; Karagianni, A.; Biswas, S.; Zaleski, C. M.; Kampf, J.; Yoder, D.; Penner-Hahn, J. E.; Pecoraro, V. L.; Kessissoglou, D. P. *Inorg. Chem.* **2003**, *42*, 2185−2187. (i) Schake, A. R.; Schmitt, E. A.; Conti, A. J.; Streib, W. E.; Huffman, J. C.; Hendrickson, D. N.; Christou, G. *Inorg. Chem.* **1991**, *30*, 3192−3199.

(21) (a) Boston, D. R.; Rose, N. J. *J. Am. Chem. Soc.* **1968**, *90*, 6859−6860. (b) Parks, J. E.; Wagner, B. E.; Holm, R. H. *J. Am. Chem. Soc.* **1970**, *92*, 3500−3502. (c) Churchill, M. R.; Reis, A. H. *Chem. Commun.* **1970**, 879−880. (d) Zakrzewski, G. A.; Ghilardi, C. A.; Lingafelter, E. C. *J. Am. Chem. Soc.* **1971**, *93*, 4411−4415. (e) Rai, H. C.; Jena, A. K.; Sahoo, B. *Inorg. Chim. Acta* **1979**, *35*, 29−33. (f) See, R. F.; Churchill, M. R.; Lance, K. A.; Mersman, D. P.; Williams, K. R. *Inorg. Chim. Acta* **1997**, *257*, 285−290. (g) Voloshin, Y. Z.; Varzatskii, O. A.; Kron, T. E.; Belsky, V. K.; Zavodnik, V. E.; Strizhakova, N. G.; Palchik, A. V. *Inorg. Chem.* **2000**, *39*, 1907−1918. (h) Engtrakul, C.; Shoemaker, W. J.; Grzybowski, J. J.; Guzei, I.; Rheingold, A. *Inorg. Chem.* **2000**, *39*, 5161−5163. (i) Kubow, S. A.; Takeuchi, K. J.; Grzybowski, J. J.; Jircitano, A. J.; Goedken, V. L. *Inorg. Chim. Acta* **1996**, *241*, 21−30.

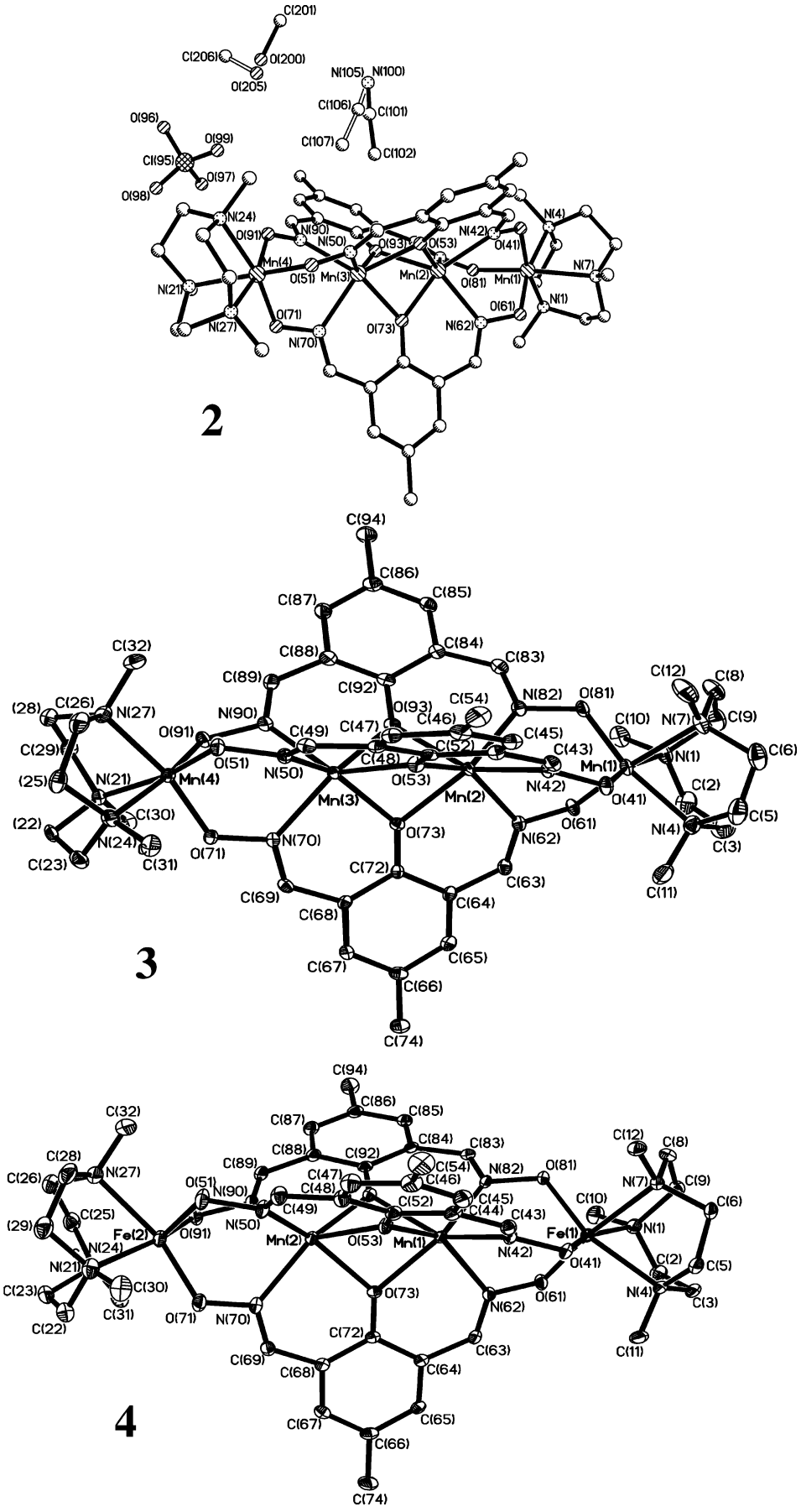

Figure 4. Molecular structures of the cations in complexes **2**, **3**, and **4**.

Table 3. Selected Bond Lengths (Å) and Angles (deg) for $Mn^{III}Mn^{II}Mn^{II}Mn^{III}$, **2**

Mn(1)···Mn(2)	3.541	Mn(2)···Mn(3)	3.043
Mn(3)···Mn(4)	3.547	Mn(1)···Mn(4)	10.129
Mn(1)−N(1)	2.134(7)	Mn(4)−N(21)	2.248(9)
Mn(1)−N(4)	2.119(8)	Mn(4)−N(24)	2.229(8)
Mn(1)−N(7)	2.315(8)	Mn(4)−N(27)	2.121(8)
Mn(1)−O(41)	1.888(6)	Mn(4)−O(51)	1.976(7)
Mn(1)−O(61)	1.894(6)	Mn(4)−O(71)	1.977(7)
Mn(1)−O(81)	2.063(7)	Mn(4)−O(91)	1.866(7)
Mn(2)−N(42)	2.214(8)	Mn(3)−N(50)	2.225(8)
Mn(2)−N(62)	2.231(8)	Mn(3)−N(70)	2.230(8)
Mn(2)−N(82)	2.196(8)	Mn(3)−N(90)	2.214(8)
Mn(2)−O(73)	2.200(6)	Mn(3)−O(73)	2.170(6)
Mn(2)−O(93)	2.176(6)	Mn(3)−O(93)	2.176(6)
Mn(2)−O(53)	2.191(6)	Mn(3)−O(53)	2.186(6)
		Mn(2)−O(53)−Mn(3)	88.1(2)
		Mn(2)−O(73)−Mn(3)	88.3(2)
		Mn(2)−O(93)−Mn(3)	88.7(2)

Table 4. Selected Bond Lengths (Å) and Angles (deg) for $Mn^{IV}Mn^{II}Mn^{II}Mn^{IV}$, **3**

Mn(1)···Mn(2)	3.538	Mn(2)···Mn(3)	2.947
Mn(3)···Mn(4)	3.537	Mn(1)···Mn(4)	10.023
Mn(1)−N(1)	2.092(4)	Mn(4)−N(21)	2.090(4)
Mn(1)−N(4)	2.096(5)	Mn(4)−N(24)	2.087(4)
Mn(1)−N(7)	2.084(4)	Mn(4)−N(27)	2.093(4)
Mn(1)−O(41)	1.847(3)	Mn(4)−O(51)	1.837(3)
Mn(1)−O(61)	1.857(4)	Mn(4)−O(71)	1.846(3)
Mn(1)−O(81)	1.841(4)	Mn(4)−O(91)	1.862(3)
Mn(2)−N(42)	2.191(4)	Mn(3)−N(50)	2.202(4)
Mn(2)−N(62)	2.192(4)	Mn(3)−N(70)	2.204(4)
Mn(2)−N(82)	2.200(4)	Mn(3)−N(90)	2.188(4)
Mn(2)−O(53)	2.156(3)	Mn(3)−O(53)	2.146(3)
Mn(2)−O(73)	2.158(3)	Mn(3)−O(73)	2.142(3)
Mn(2)−O(93)	2.141(3)	Mn(3)−O(93)	2.175(3)
		Mn(2)−O(53)−Mn(3)	86.49(12)
		Mn(2)−O(73)−Mn(3)	86.54(12)
		Mn(2)−O(93)−Mn(3)	86.14(12)

supporting the high-spin d^5 configuration for the terminal ions.[6,16] Additional support for the assignment comes from the Mössbauer parameters, described earlier. The intramolecular Fe(1)···Fe(2) separation is 10.034 Å for **4**.

The Mn−O and Mn−N bond lengths for the central dimanganese core, i.e., Mn(2) and Mn(3) atoms for complexes **2**, **3**, and **4**, fall in the range of 2.141(3)−2.200(6) Å for Mn−O(phenoxo) and 2.214(8)−2.245(2) Å for Mn−N(oxime), which are completely in accord with a high-spin d^5 electron configuration described in the literature for comparable structures.[14b,17,18] Thus, like the corresponding tris-(μ-phenoxo)dimanganese(II) core in complex **1**, the central dimanganese face-shared bioctahedron in **2**−**4** is severely distorted. The coordination polyhedron around manganese(II) centers in complexes **2**−**4** is not an ideal trigonal prism with trigonal twist angles of average 11.5° for **2**, 8.7° for **3**, and 10.5° for **4** and is thus slightly distorted toward an octahedron (trigonal twist angle: 60° for an octahedron and 0° for a trigonal prismatic arrangement). The average trigonal twist angle is 0.8° for **1**. Summarily, the conformations of the dimanganese(II) confacial bioctahedra for complexes **1**−**4** are essentially identical with one another.

For comparison purposes, important structural parameters are given in Table 6. Our attempts to grow X-ray quality crystals of complex **5** for the structure determination failed.

Table 5. Selected Bond Lengths (Å) and Angles (deg) for $Fe^{III}Mn^{II}Mn^{II}Fe^{III}$, **4**

Fe(1)···Mn(2)	3.507	Mn(2)···Mn(3)	3.029
Mn(3)···Fe(4)	3.498	Fe(1)···Fe(4)	10.034
Fe(1)−N(1)	2.239(3)	Fe(4)−N(21)	2.226(2)
Fe(1)−N(4)	2.232(2)	Fe(4)−N(24)	2.234(3)
Fe(1)−N(7)	2.226(2)	Fe(4)−N(27)	2.230(3)
Fe(1)−O(41)	1.938(2)	Fe(4)−O(51)	1.907(2)
Fe(1)−O(61)	1.935(2)	Fe(4)−O(71)	1.927(2)
Fe(1)−O(81)	1.917(2)	Fe(4)−O(91)	1.923(2)
Mn(2)−N(42)	2.228(2)	Mn(3)−N(50)	2.206(2)
Mn(2)−N(62)	2.245(2)	Mn(3)−N(70)	2.224(2)
Mn(2)−N(82)	2.192(2)	Mn(3)−N(90)	2.229(2)
Mn(2)−O(53)	2.170(2)	Mn(3)−O(53)	2.193(2)
Mn(2)−O(73)	2.179(2)	Mn(3)−O(73)	2.177(2)
Mn(2)−O(93)	2.194(2)	Mn(3)−O(93)	2.174(2)
		Mn(2)−O(53)−Mn(3)	87.92(7)
		Mn(2)−O(73)−Mn(3)	88.12(7)
		Mn(2)−O(93)−Mn(3)	87.82(7)

Table 6. Important Structural Parameters for Complexes **1**−**4**

complex	twist angles, ϕ (deg)[a]	dihedral angles, θ (deg)[b]
1, $B^{III}Mn^{II}Mn^{II}B^{III}$	1.2/1.1/0	4.3/5.8/6.7
2, $Mn^{III}Mn^{II}Mn^{II}Mn^{III}$	8.4/11.4/11.8	35.7/33.0/34.1
	12.8/12.0/13.1	31.1/30.0/30.0
3, $Mn^{IV}Mn^{II}Mn^{II}Mn^{IV}$	8.8/8.1/12.3	37.9/27.7/39.8
	8.7/5.0/9.2	20.8/27.1/34.3
4, $Fe^{III}Mn^{II}Mn^{II}Fe^{III}$	10.7/10.0/10.8	32.5/29.9/34.0
		31.5/29.0/29.0

[a] The trigonal twist angle, ϕ, is the angle between the triangular faces comprising three oximate N atoms and three phenolate O atoms and has been calculated as the Newman projection angles viewed along the centroids of focus. For an ideal trigonal prismatic arrangement, ϕ is 0° and 60° for an octahedron. [b] That the core $M_t(O-N)Mn^{II}$ is not linear is shown by the dihedral angles, θ, between the planes comprising $M_t(O-N)$ and $Mn^{II}(N-O)$ atoms.

Magnetic Properties. Magnetic susceptibility data for polycrystalline samples of complexes **1**−**5** were collected in the temperature range 2−290 K in an applied magnetic field of 1 T not only to characterize the nature and magnitude of the exchange interaction propagated by the bridging oximate and phenoxide ligands but also to find out the influence of terminal metal ions on the exchange coupling between the central manganese(II) centers. We use the Heisenberg spin Hamiltonian in the form $H = -2J\hat{S}_i\cdot\hat{S}_J$ for an isotropic exchange coupling with $S_{Mn} = {}^5/_2$ and $S_B = 0$ for **1**, with $S_{Mn(III)} = {}^4/_2$ and $S_{Mn} = {}^5/_2$ for **2**, with $S_{Mn(IV)} = {}^3/_2$ and $S_{Mn} = {}^5/_2$ for **3**, with $S_{Fe} = {}^5/_2$ and $S_{Mn} = {}^5/_2$ for **4**, and $S_{Cr} = {}^3/_2$ and $S_{Mn} = {}^5/_2$ for **5**. The experimental magnetic data were simulated using a least-squares fitting computer program with a full-matrix diagonalization of exchange coupling, Zeeman splitting, and axial single-ion zero-field interaction (DS_z^2), if necessary. The experimental data and their simulations as solid lines are displayed in Figure 5.

The magnetic moment, μ_{eff}/molecule, for **1**, $B^{III}Mn^{II}Mn^{II}B^{III}$, of 7.13 μ_B ($\chi_M T = 6.353$ cm^3 K mol^{-1}) at 290 K decreases monotonically with decreasing temperature until it reaches a value of 0.74 μ_B ($\chi_M T = 0.0677$ cm^3 K mol^{-1}) at 2 K; this temperature dependence of μ_{eff} is a clear indication of an antiferromagnetic exchange coupling between two paramagnetic centers Mn(II) ($S = {}^5/_2$) with a resulting $S_t = 0$ ground state. The solid line in Figure 5 represents

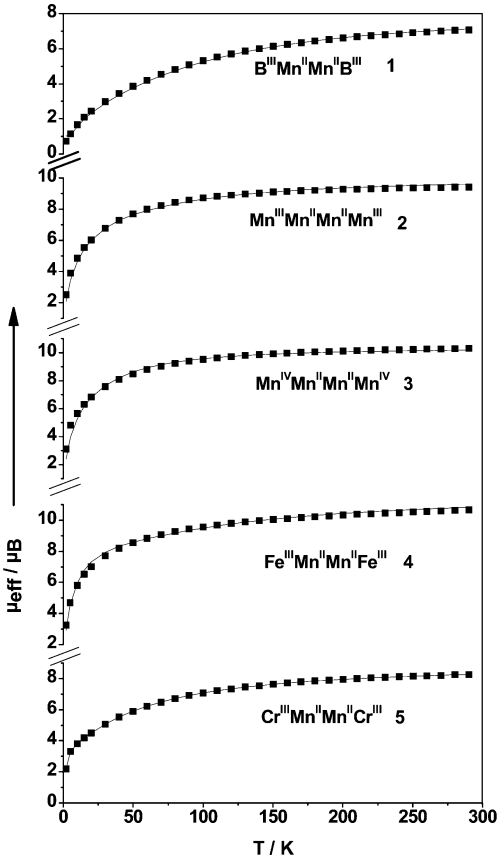

Figure 5. Temperature dependence of the magnetic moments of complexes **1**−**5**. The solid lines represent the best fit of the data to the Heisenberg−Dirac−van Vleck model (see text).

the best fit with the following parameters: $J = -9.1$ cm^{-1}, $g = 2.00$, and PI ($S = {}^5/_2$) = 3%.

These new data now permit an examination of exchange coupling in dimanganese(II) systems in which the number of bridging phenoxo groups increases from one to three. To the best of our knowledge, no structural and magnetic data exist for singly bridged mono(μ-phenoxo) $Mn_2(\mu_2$-OPh) and tris(μ-phenoxo)-bridged $Mn_2(\mu_2$-OPh)$_3$ dimanganese(II) complexes, although several dinuclear manganese(II) complexes containing the μ-phenolato-bis(μ-carboxylato) core structure are known[20e,f] to exhibit antiferromagnetic exchange coupling (−5 to −11 cm^{-1}). Exchange coupling constants in bis(μ-phenoxo)-bridged dimanganese(II) complexes published[20] have been found to be very small, lying in a small range of +0.2 to −1.88 cm^{-1}. It is worth pointing out that the bridging phenoxide Mn−O−Mn angles do *not* seem to correlate with the magnitude of J. The angle at the bridging phenoxide oxygen would be expected to be important, as this affects the nature of σ and π overlap between the manganese magnetic orbitals and the oxygen p_x, p_y, and p_z orbitals that mediate the exchange interaction. The presence of three monatomic phenoxide bridges in **1**, $B^{III}Mn^{II}Mn^{II}B^{III}$, results in smaller angles (86.0−86.7°) compared to those of the other complexes, which possess only one (100−116°) (monophenoxide bridge together with two additional carboxylato bridges) or only two phenoxide bridges (av 101°). The smaller Mn−O−Mn angles in **1** would be expected to increase the contribution to J from ferromagnetic pathways due to the resulting near orthogonality of some of the magnetic orbitals. In contrast to this analysis, the tris(μ-phenoxo)-bridged dimanganese(II) compound, $B^{III}Mn^{II}Mn^{I}{}_{I}B^{III}$, **1** exhibits the largest antiferromagnetic exchange coupling constant yet observed in only phenoxide-bridged dimanganese(II) complexes, probably as a result of the number of bridging ligands and deviation of the metal geometry to a trigonal prism (D_{3h}).

Scheme 2

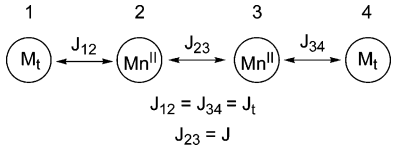

Table 7. Magnetic Parameters Obtained from the Data at 1 T for Complexes **1**−**5**

no.	complex	J_t, cm^{-1} ($J_{12} = J_{34}$)	J_{23}, cm^{-1}	$g_{Mn(II)}$ (fixed)	g_t (fixed)
1	$B^{III}Mn^{II}Mn^{II}B^{III}$	−	−9.1	2.00	−
2	$Mn^{III}Mn^{II}Mn^{II}Mn^{III}$	+2.4	−9.1 (fixed)	2.00	1.9
3	$Mn^{IV}Mn^{II}Mn^{II}Mn^{IV}$	+2.5	−4.1	2.00	2.00
4	$Fe^{III}Mn^{II}Mn^{II}Fe^{III}$	−1.45	−9.1 (fixed)	2.00	2.00
5	$Cr^{III}Mn^{II}Mn^{II}Cr^{III}$	−2.2	−9.1 (fixed)	2.00	1.90

The magnetic moments, μ_{eff}/molecule, for **2**−**5** decrease monotonically with decreasing temperature, clearly indicating a predominance of antiferromagnetic exchange coupling in these complexes (Figure 5). As the nature of the temperature dependence of the magnetic moments μ_{eff} for **2**−**5** can be immediately seen from Figure 5, but not easily the exact μ_{eff} values, selected values are supplied as Supporting Information (Table S1). The magnetic analysis was carried out using the model shown in Scheme 2.

In this model, J_{ik} represents the exchange interaction between the ith and kth paramagnetic ions; thus, $J_{12} = J_{34}$ describes the interaction between the terminal trivalent or tetravalent ions and the adjacent manganese(II) ions, J_{23} the interaction between the neighboring central manganese(II) ions. To avoid overparametrization, we have used the simplest model, viz. a two-J model. The interactions J_{13}, J_{24}, and J_{14} the interaction between the terminal ions were not considered, as the corresponding distances ~7 and 10 Å, respectively, are too long for any significant exchange interaction.

As the conformations of the dimanganese(II) confacial biooctahedra for complexes **1**−**4** are essentially identical with one another and complex **1** is magnetically only a dinuclear Mn(II) complex, we have used the intradimanganese(II) coupling $J = J_{23} = -9.1$ cm^{-1} for the least-squares fitting of the data for **2**−**5** to the model in Scheme 2. Thus, the following constraints are used for simulation of the experimental data for complexes **2**−**5**: $g_{Mn(II)} = 2.0$ (fixed), $J_{23} = J = -9.1$ cm^{-1} (fixed). The simulated magnetic parameters are listed in Table 7. It is to be mentioned that all our attempts to use the constraint $J_{23} = J = -9.1$ cm^{-1} (fixed) for **3**, $Mn^{IV}Mn^{II}Mn^{II}Mn^{IV}$, failed to reproduce the observed data for **3**. Thus, the parameters J_t and J were allowed to float

Table 8. Unbiassed Best Fit Results Obtained from the Data at 1 T for Complexes **1**−**5**

complex[a]	J_t, cm^{-1}, (J_{12}=J_{34})	J, cm^{-1}, (J_{23})
1, $B^{III}Mn^{II}Mn^{II}B^{III}$	−	−9.1
2, $Mn^{III}Mn^{II}Mn^{II}Mn^{III}$	+2.8	−8.2
3, $Mn^{IV}Mn^{II}Mn^{II}Mn^{IV}$	+2.5	−4.1
4, $Fe^{III}Mn^{II}Mn^{II}Fe^{III}$	−1.8	−8.0
5, $Cr^{III}Mn^{II}Mn^{II}Cr^{III}$	−2.4	−8.75

[a] $g_{Mn(II)} = 2.00$ was kept fixed for **2**−**5**. $g_{Mn(III)} = 1.90$ (fixed) for **2**. $g_{Mn(IV)} = 2.00$ (fixed) for **3**. $g_{Fe(III)} = 2.00$ (fixed) for **4**. $g_{Cr(III)} = 1.90$ (fixed) for **5**.

during the simulation and the following fitting parameters were obtained for **3**: $J_{12} = J_{34} = J_t = +2.5$ cm^{-1}, $J_{23} = J = -4.1$ cm^{-1}, $g_{Mn(IV)} = 2.0$ (fixed), $g_{Mn(II)} = 2.0$ (fixed). Similarly, the magnetic data for **2**, **4**, and **5** were subjected to least-squares fitting without the constraint of $J = -9.1$ cm^{-1} (fixed). These unbiased fitting results are listed in Table 8. We have kept the *g* factors fixed to realistic values to avoid over parametrization. These unbiased best fit results indicate two remarkable points: (i) the intra-dimanganese-(II) couplings, *J*, for **2**, **4**, and **5** span within a small range of −8.0 to −8.75 cm^{-1} and are very similar to that with $J = -9.1$ cm^{-1} for **1**, $B^{III}Mn^{II}Mn^{II}B^{III}$, which is magnetically easier to handle because of the presence of only two paramagnetic centers; thus, the results listed in Tables 7 and 8 indicate clearly that the terminal trivalent paramagnetic metal ions such as Cr^{III}, Mn^{III}, and Fe^{III} have insignificant influence on the coupling operating between the central manganese(II) centers; (ii) on the other hand, the terminal tetravalent Mn^{IV} ions influence the intra-dimanganese(II) coupling; the parameter *J* for **3** is significantly weaker with $J = -4.1$ cm^{-1} in comparison to those for **2**, **4**, and **5**.

To determine whether the fit for **3** is unique, a search in the form of a relative error surface for fitting the measured data by the theoretical expression was performed. In Figure 6 is shown a three-dimensional and a two-dimensional contour projection of the relative error surface for fitting the magnetic data of complex **3** as a function of both J_t and *J*. Only the region of smallest relative error is presented. It can be concluded that the above parameters lie well in a global minimum in the parameter space for this system and allow us to estimate the approximate error bars on the J_t and *J* values: $J_t = +3 \pm 1$ cm^{-1}, $J = -4.3 \pm 0.4$ cm^{-1}. Similarly, the global minima for other complexes were also checked.

The variable-field (1, 4, and 7 T) variable-temperature (2−5 K) reduced magnetization data were analyzed including, in addition to the above J_t, *J*, and *g* variables, the axial zero-field splitting parameter, D_t, for the terminal metal ions. Analysis of the data using an axial zero-field splitting model is potentially very complex since the closely spaced levels of $S_t = 0$, 1, 2, 3, etc. (within ca. 10 cm^{-1}) will undergo splitting and crossing. To try and simplify the situation, an approximate approach of considering different parameters at different field strengths was used. It is very gratifying to observe that the fitting parameters do not differ drastically from the values listed in Tables 7 and 8. Table 9 summarizes the VTVH data for complexes **2**−**4**. We want to stress that

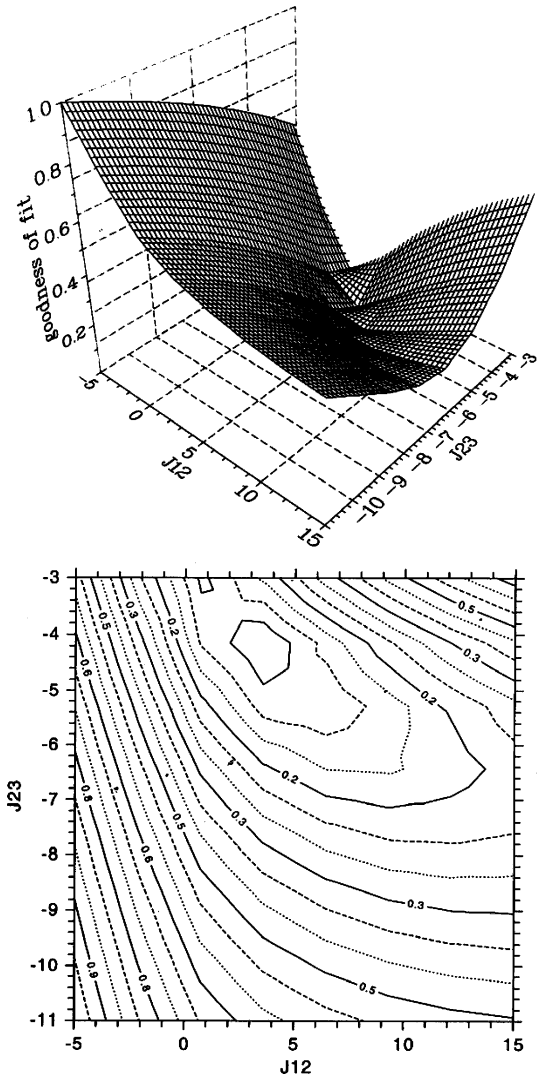

Figure 6. 3D- and 2D-contour projections of the relative error surface for fitting the magnetic data of complex **3**.

Table 9. Parameters Obtained from the VTVH Magnetization Measurements for Complexes **2**−**4**[a]

no.	complex	J_t, cm^{-1}	*J*, cm^{-1}	D_t, cm^{-1}	g_t (fixed)
2	$Mn^{III}Mn^{II}Mn^{II}Mn^{III}$ at 1 T	+1.4	−9.1 (fixed)	−1.1	1.89
	$Mn^{III}Mn^{II}Mn^{II}Mn^{III}$ at 4 T	+2.45	−9.1 (fixed)	−1.0	1.89
	$Mn^{III}Mn^{II}Mn^{II}Mn^{III}$ at 7 T	+3.4	−9.1 (fixed)	−1.0	1.89
3	$Mn^{IV}Mn^{II}Mn^{II}Mn^{IV}$ at 1 T	+1.9	−4.1	|0.2|	2.00
	$Mn^{IV}Mn^{II}Mn^{II}Mn^{IV}$ at 4 T	+2.3	−4.1	|0.3|	2.00
	$Mn^{IV}Mn^{II}Mn^{II}Mn^{IV}$ at 7 T	+2.4	−4.1	|0.3|	2.00
4	$Fe^{III}Mn^{II}Mn^{II}Fe^{III}$ at 1 T	−1.3	−9.1 (fixed)	|0.2|	2.00
	$Fe^{III}Mn^{II}Mn^{II}Fe^{III}$ at 2 T	−1.5	−9.1 (fixed)	|0.2|	2.00
	$Fe^{III}Mn^{II}Mn^{II}Fe^{III}$ at 4 T	−1.8	−9.1 (fixed)	|0.2|	2.00
	$Fe^{III}Mn^{II}Mn^{II}Fe^{III}$	−2.0	−9.1 (fixed)	|0.2|	2.00

[a] $g_{Mn(II)} = 2.00$ was kept fixed for **2**−**4**.

for **2** the fit with D_t being negative is markedly superior to D_t being positive and hence the negative *D* value is strongly favored. In contrast, for complexes **3**−**4**, the sign of D_t has no influence on the quality of the fit. The simulated curves for the VTVH measurements are included as Supporting Information (Figures S1, S2, S3).

We would try to analyze the exchange parameters by considering the idealized sp^2 hybridization of the O and N atoms of the bridging oxime groups, through which the different metal d orbitals interact with each other. The bridge network $M_t(O-N)_3Mn^{II}$ as a whole possesses an idealized D_{3h} symmetry. The five metal d orbitals, with the 3-fold axis as the axis of highest symmetry, *z* axis, transform as a'_1-(d_{z^2}), e″(d_{xz}, d_{yz}) and e′($d_{x^2-y^2}$, d_{xy}).

It is clear from Table 8 that the coupling J_t between the centers $Mn^{III}\cdots Mn^{II}$ in **2** and $Mn^{IV}\cdots Mn^{II}$ in **3** is weakly ferromagnetic. Such ferromagnetic coupling between the mentioned centers is known in the oximate-bridged complexes.[15] For complexes **2**, $Mn^{III}(d^4$ hs)$Mn^{II}(d^5$ hs), and **3**, $Mn^{IV}(d^3)Mn^{II}(d^5$ hs), it is evident that the contribution of the path e′||sp^2||e′ (using Ginsberg's symbols)[22] to the overall interaction, J_t, becomes dominant, since the e′ orbitals centered on Mn(III) or Mn(IV) are occupied by one electron or are empty, respectively, whereas the same orbitals on Mn-(II) are singly occupied. An overall ferromagnetic interaction, albeit weak, is therefore not unexpected and has been observed, also earlier in the manganese chemistry.[20i] Interestingly, the Cr(III)-containing compound **5**, which is isoelectronic with compound **3**, exhibits weak antiferromagnetic $Cr^{III}\cdots Mn^{II}$ interaction, as has been described earlier in the literature.[23] This change in the nature of the observed coupling ($J_{exp} = J_{AF} + J_F$) is presumably due to the subtle changes in the individual ferromagnetic and antiferromagnetic contributions to the overall coupling and can be attributed to the high positive charge on the manganese(IV) center in **3** in comparison to that in **5** with a lower charge on Cr(III). This effect of charge has also a profound influence on the coupling between the central manganese(II) centers, as is evident from Table 8.

The deviation of the core $M_t(O-N)Mn^{II}$ from linearity (Table 6) is most apparent for complex **3** containing the Mn-(IV) centers as terminal M_t ions due to the tendency of d^3 electronic configuration to exhibit more rigid regular octahedral geometry, in comparison to more flexible geometry for d^4 and d^5 electronic configurations. Thus, the dimanganese(II) cores in **3** and **5** are more prone to distortion from trigonal prism toward octahedron, tending the splitting of the d orbitals qualitatively in only two orthogonal energy levels and hence increasing the ferromagnetic contributions to overall exchange coupling. As a result, a reduction in the strength of antiferromagnetic interaction $J_{23} = J$ in **3** is observed. This reduction is visualized for **3** containing Mn-(IV) but not for **5** containing the Cr(III) ions, as more covalent nature of the M−oxime bonds prevailing in **3** with Mn(IV) facilitates the exchange coupling more easily in comparison to that in **5** containing the lower-charged Cr(III). Thus, the distortion of the central metal ions from the trigonal prismatic arrangements of the ligands toward an octahedron acts as a barrier toward the antiferromagnetic spin coupling, which is a result of the covalent interaction between the orbitals of the oxime network and the terminal metal ions.

Concluding Remarks

To conclude, the following points of this study deserve particular attention:

(i) The dinucleating oxime, 2,6-diformyl-4-methylphenol oxime, H_3dfmp, is as expected capable of forming with divalent transition metal ions dimetallic building blocks $[M^{II}_2(dfmp)_3]^{5-}$, which can act as ligands to give rise to various linear tetranuclear complexes of the type M_AM_B-M_BM_A, in which the central metal ions M_B's are embedded in the dinucleating phenol-oxime ligand. The central metal ions M_B's are bridged through three phenoxo ligands, thus yielding a face-shared bioctahedron for the divalent metal ions, M_B. The terminal metal ions, M_A, are triply bridged through three oximato groups (−O═N−) to the neighboring M_B, thus assembling molecules with four magnetic subunits in a linear fashion. Because of their isostructural nature, these materials are unique and ideally suited for the study of intramolecular exchange interactions between four paramagnetic transition metal ions as a function of their respective d^n electron configurations.

(ii) Two isoelectronic isostructural compounds, $Mn^{IV}Mn^{II}$ **3** and $Cr^{III}Mn^{II}$ **5**, with d^3d^5(hs) electronic configurations exhibit different spin coupling, ferromagnetic for **3**, but antiferromagnetic for **5**. The prevailing competing symmetry-related interactions, viz. $t_{2g}^3 \perp e'g^2$ and $t_{2g}^3||t'_{2g}^3$ in **3** and **5** lead to the observed results of exchange interactions opposite in nature for the triply oximato-bridged six-coordinate M_AM_B systems, presumably due to the mixing of five metal d orbitals in trigonal symmetry, which provides several exchange components opposite in nature; thus, a bulk weak but opposite exchange interactions result. Ferromagnetic interactions in **3** with Mn(IV) can be attributed to the more covalent nature of the Mn(IV)−oxime bonds in comparison to those in **5** containing the lower-charged Cr(III). We will continue with our attempts to gather structural data for **5** and to discern the mechanism through which the covalency of Mn(IV)−oxime bond affects the exchange-coupling interaction within the dimanganese(II) unit.

(iii) An interesting and unusual result emerges from the comparison of the spin interactions within the dimanganese-(II) units in **3** and **5** (Table 8). Higher charge of terminal Mn(IV) in **3** has a profound influence on the exchange coupling prevailing in the central trisphenoxodimanganese(II) core by increasing the ferromagnetic components to the overall exchange. Thus, the strength of the exchange coupling in **3** diminishes to $-J_{23} = 4.1$ cm^{-1} from 9.1 cm^{-1} for **1**, **2**, **4**, and **5**.

It is noteworthy that the average angle at the bridging phenoxo groups for the central dimanganese(II) Mn−O(phenoxo)−Mn is identical for **1** and **3** (86.3°); thus, no

(22) Ginsberg, A. P. *Inorg. Chim. Acta Rev.* **1971**, *5*, 45.
(23) For example: (a) Chaudhuri, P.; Winter, M.; Küppers, H. J.; Wieghardt, K.; Nuber, B.; Weiss, J. *Inorg. Chem.* **1987**, *26*, 3302−3310. (b) Corbin, K. M.; Gleurup, J.; Hodgson, D. L.; Lynn, M. H.; Michelsen, K.; Nielsen, K. M. *Inorg. Chem.* **1993**, *32*, 18−26. (c) Marinescu, G.; Visinescu, D.; Cucos, A.; Andruh, M.; Journaux, Y.; Kravtsov, V.; Simonov, Y. A.; Lipkowski, J. *Eur. J. Inorg. Chem.* **2004**, 2914−2922. (d) Ni, Z.-H.; Kou, H. Z.; Zheng, L.; Zhao, Y. H.; Zhang, L. F.; Wang, R. J.; Cui, A. L.; Sato, O. *Inorg. Chem.* **2005**, *44*, 4728−4736. (e) Bonadio, F.; Senna, M. C.; Ensling, J.; Sieber, A.; Neels, A.; Stoeckli-Evans, H.; Decurtins, S. *Inorg. Chem.* **2005**, *44*, 969−978.

simple angle-dependent correlation of the exchange coupling for the trisphenoxodimanganese(II) unit is expected.

(iv) Although linear tetranuclear complexes of this type are not good candidates for generating molecules with high spins, they are ideally suited for studying systematically influence of terminal metal ions on the exchange coupling.

(v) That terminal Mn(IV) ions in comparison to Cr(III) ions reduce the overall antiferromagnetic exchange between the central Mn(II) ions is an important experimental information.

Acknowledgment. Financial support from the Max-Planck Society and the German Research Foundation (DFG) (Priority Program "Molecular Magnetism") is gratefully acknowledged.

Supporting Information Available: Table S1 and Figures S1−S3 and X-ray crystallographic files in CIF format. This material is available free of charge via the Internet at http://pubs.acs.org.

IC060409A